Interactions of Carboplatin and Oxaliplatin with Proteins: Insights from X-ray structures and mass spectrometry studies of their Ribonuclease A adducts

Luigi Messori,[a,*] Tiziano Marzo,[a] and Antonello Merlino*[,b,c]

[a]Department of Chemistry, University of Florence, Via della Lastruccia 3, 50019, Sesto Fiorentino, Italy

[b]Department of Chemical Sciences, University of Naples Federico II, Complesso Universitario di Monte Sant' Angelo Via Cintia, I-80126, Napoli, Italy

[c]CNR Institute of Biostructures and Bioimages, Via Mezzocannone 16, I-80100, Napoli, Italy

*Corresponding authors:

Antonello Merlino,

Department of Chemical Sciences, University of Naples 'Federico II', via Cintia, 80126, Napoli, Italy

Tel: +39-081674276; fax: +39-081674090.

E-mail address: antonello.merlino@unina.it

and

Luigi Messori

Department of Chemistry, University of Florence, Via della Lastruccia 3, 50019, Sesto Fiorentino, Italy

Tel: +39- 055 4573388; fax: +39-055 4574913.

E-mail address: luigi.messori@unifi.it

Keywords: Cancer, Platinum, Medicinal Chemistry, Mass Spectrometry, X-ray crystallography.

Abstract

Oxaliplatin and carboplatin are two platinum(II) drugs in widespread clinical use for the treatment of various types of cancers; yet, structural information on their interactions with proteins is scarce. Here, the X-ray structures of the adducts formed upon reaction of carboplatin and oxaliplatin with bovine pancreatic ribonuclease (RNase A) are reported and compared with results obtained for the structure of the RNase A-cisplatin adduct derived from isomorphous crystals, under the same experimental conditions. Additional details on the binding mode of these metallodrugs toward RNase A are provided by Electrospray Ionisation Mass Spectrometry (ESI MS) measurements, thus offering insight on the occurring metal-protein interactions. Notably, while carboplatin and cisplatin mainly bind the side chain of Met29, oxaliplatin also binds the side chains of Asp14, of catalytically important His119 and, to a lesser extent, of His105. On the basis of the available data, a likely mechanism for oxaliplatin hydrolysis and binding to the protein is proposed. These results are potentially useful for a better understanding of the biological chemistry, toxicity and side effects of this important class of antitumor agents.

1. Introduction

Cisplatin (cis-diamminedichloroplatinum(II), Figure 1) is one of the most potent anticancer drugs in established clinical use for the treatment of several kinds of cancer [1-2]. Carboplatin and oxaliplatin (Figure 1) are two cisplatin analogs that are widely used in cancer therapeutics either as an alternative to cisplatin (carboplatin) or for cancer types that are poorly responsive to cisplatin (oxaliplatin) [3-5]. Apparently, these metallodrugs exert their effects mainly by interfering with the DNA replication and transcription machinery through formation of adducts with nuclear DNA; however their specific pharmacological profiles appear to be quite distinct [6-7]. Beyond their mechanistically relevant DNA interactions, cisplatin, carboplatin and oxaliplatin (Figure 1) have been implicated in extensive formation of Pt-protein adducts. Though the involvement of these adducts in the mode of action and toxicity of Pt drugs is still unclear, more and more attention is being placed upon protein-Pt drugs interactions in relation to their overall pharmacological and toxicological impact [8-11]. Yet, the structural information concerning the interactions of platinum drugs with proteins and the characterization of the resulting adducts is quite limited [8-11]. In particular, while the interaction between cisplatin and proteins is underscored by a number of biochemical, biophysical and structural studies [12-20], the formation of oxaliplatin and carboplatin-protein adducts is far less explored and understood [21-24].

Figure 1

From the crystallographic point of view, formation of complexes between cisplatin and hen egg white lysozyme (HEWL) [12], the copper chaperone Atox-1 [13], bovine erythrocyte Cu, Zn superoxide dismutase (beSOD) [14], bovine pancreatic ribonuclease (RNase A) [15], human superoxide dismutase [16], horse heart cytochrome c [17], Na+/K+-ATPase [18] and human serum albumin [19] has been studied. On the other hand, the only structures known for the other two Pt drugs are those of their adducts with HEWL [21-24].

The structure of the main adduct that forms when cisplatin reacts with RNase A was recently reported [15]. This structure, which was refined at 1.85 Å resolution in the space group C2, presents two molecules in the asymmetric unit (molecule A and B). The Pt(II) center is bound to the protein in a slightly distorted square-planar arrangement and is able to form monodentate or bidentate adducts. In particular, Pt(II) can bind either to Met29 (molecule A) or to Met29 and Gln28 simultaneously (molecule B) (Figure 2A). An additional structure for RNase A-cisplatin adduct (space group $P3_221$), obtained upon crystallizing purified protein after 24 h of incubation in the presence of a large excess of cisplatin, shows that additional binding sites can be observed close to His105 and His119 [25].

RNase A was chosen as a model to study protein interactions with Pt-based [15, 20, 25, 26] and other metal drugs [27-28], since it is a stable, small, well characterized protein that is commercially available at low cost; in addition, it is easy to crystallize, forming crystals resistant to soaking under different experimental conditions. This protein is frequently used as a model system also in many other fields, including protein chemistry, enzymology, chemical synthesis and structural biology [29].

Here, we report the X-ray structures of the complexes formed when oxaliplatin or carboplatin react with RNase A. Structural data are nicely supported by independent Electrospray Ionisation Mass Spectrometry (ESI MS) measurements. Thanks to the present data, crystal structures are now available for the derivatives of the same protein with the three main platinum drugs. These structures were obtained from isomorphous crystals with two molecules in the asymmetric unit and under the same experimental conditions. Accordingly, direct structural comparisons can be done that are meaningful and instructive and may contribute to understand the molecular basis for the relevant differences in their respective pharmacological profiles.

2. Materials and Methods

2.1 Crystallization

Oxaliplatin, carboplatin and RNase A (type XII-A), sodium citrate and PEG4K were obtained from Sigma. Crystals of the RNase A adducts were obtained by soaking experiments where pre-grown monoclinic protein crystals were incubated with an excess of the platinum drug (at a protein to platinum ratio 1:10). This procedure has been already used to obtain crystals of productive complexes of RNase A including that with cisplatin [15] and other metallodrugs [26-28]. Briefly, the crystals of RNase A were grown as previously described [15,26-28] by hanging-drop vapor mixing 1 µL of RNase A at 20 mg mL^{-1} with equal volumes of reservoir solution containing 20% PEG4000 and 20 mM sodium citrate buffer pH 5.0 at 298 K. Two weeks after their appearance, crystals have been soaked for four days in a solution of carboplatin or oxaliplatin dissolved in 10 µL of reservoir. Final Pt drugs:protein concentration ratios were 10:1.

2.2 Data collection and refinement

X-ray diffraction data have been collected from single crystals at the CNR Institute of Biostructure and Bioimages, Naples, Italy, using a Saturn944 CCD detector equipped with CuKα X-ray radiation from a Rigaku Micromax 007 HF generator. Crystals have been flash-frozen at 100 K using nitrogen gas produced by an Oxford Cryosystem (and maintained at 100 K during the data collection) without using cryoprotectants, following the dehydration procedure [30] already used in many other works [31-33]. Data sets were processed and scaled using the HKL2000 package [34]. Although the soaking significantly affects the quality and the diffraction power of RNase A crystals, X-ray diffraction data have been collected at 2.09 Å and 2.27 Å resolution for carboplatin and oxaliplatin, respectively. Attempts to improve the resolution collecting datasets on crystals soaked with Pt drug with a reduced time of soaking (up to 5 hours) leads to acquisition of data corresponding to ligand-free RNase A. Data collection statistics are reported in Table S1. The structures have been solved by molecular replacement method, using the PDB file 1JVT [35], without water molecules and ligands, as starting model. The refinement was carried out with Refmac5 [36], model building and map inspections were performed using Coot [37]. 5% of the data was used for calculation of the R-free value. The initial 2Fo-Fc and Fo-Fc electron density maps clearly indicated the position of Pt ions. The binding of Carboplatin induces the disordering of residues 16-22 and of the Tyr25 side chains, which are not included in the final model. The binding of Oxaliplatin induces disordering of residues 16-23 in molecule A, 18-21 in molecule B and of Gln28 side chain. In this last structure residues 16-23 in molecule A and residues 18-19 in molecule B have been omitted from the final model, the other disordered residues (residues 16-17 and 20-21 of molecule B) are fitted in a

poor electron density Refinement statistics are reported in Table S1. Structure validation has been carried out using Procheck [38]. Coordinates and structure factors for the adducts have been deposited in the Protein Data Bank (PDB codes 4S0Q and 4S18).

2.3 Electrospray mass spectrometry

A solution of Cisplatin, carboplatin or oxaliplatin with RNase A (10^{-4} M) (3:1 metal/protein ratio) in 20 mmol L^{-1} ammonium acetate pH 6.8 was incubated at 37°C for one week and ESI MS spectra were recorded after 24, 72 h and one week. After a 20-fold dilution with water, ESI MS spectra have been recorded by direct introduction at 5 µl min^{-1} flow rate in an Orbitrap high-resolution mass spectrometer (Thermo, San Jose, CA, USA), equipped with a conventional ESI source. The working conditions were the following: spray voltage 3.1 kV, capillary voltage 45 V, capillary temperature 220°C, tube lens voltage 230 V. The sheath and the auxiliary gases were set, respectively, at 17 (arbitrary units) and 1 (arbitrary units). For acquisition, Xcalibur 2.0. software (Thermo) was used and monoisotopic and average deconvoluted masses were obtained by using the integrated -Xtract tool. For spectrum acquisition, a nominal resolution (at m/z 400) of 100,000 was used.

3. **Results**

3.1 Crystal structures

The structures of RNase A-carboplatin and RNase A-oxaliplatin have been solved at 2.09 and 2.27 Å resolution, respectively. The overall structures of the two adducts are reported in Figure 2 B and 2C. The structures have been refined to Rfactor=20.5 and 22.4 (Rfree=26.2 and 30.1), for the RNase A complexes with carboplatin and oxaliplatin, respectively. In both structures, the electron density maps of protein regions are rather well defined, with exceptions consisting of a few portions in both the molecules present in the asymmetric unit (molecule A and B, hereafter) of the two complexes. Similarly to what found for the RNase A-cisplatin complex [15] (Figure 2A), in both RNase A-carboplatin and RNase A-oxaliplatin adducts platination does not affect the overall conformation of the protein, which remains very similar to the wild-type (CA root mean square deviations in the range 0.36-0.60 Å).

Figure 2

As previously found for cisplatin [15] and chloroplatinite ($PtCl_4^{2-}$) [20], the RNase A-carboplatin interaction in both A and B molecules mainly occurs at the SD atom of the side chain of Met29. However, due to unclear electron density maps likely associated with low occupancy and to the possible conformational disorder of this site, the local environment of the bound Pt(II) center, in the RNase A-carboplatin adduct, could not be unambiguously determined (Figure 3A and B). The refinement of B-factors of Pt ligands and the inspection of residual Fo-Fc electron density maps suggests that the Pt ions have occupancy= 0.50 and 0.35 for molecule A and B, respectively. In both these chains, platination of Met29 induces a disordering of residue 16-22 and of Tyr25 side chain.

Figure 3

Although crystals of RNase A-oxaliplatin diffract to a resolution slightly lower than that obtained for RNase A-carboplatin and RNase A-cisplatin [15] complexes, the electron density maps clearly reveal details of the binding. In the RNase A-oxaliplatin structure, six Pt binding sites have been identified, i.e. three binding sites for each molecule of the asymmetric unit.

In the main oxaliplatin binding site, the Pt(II) ion is bound to ND1 atom of His119 (Figure 4A and B). In this site, the electron density map is well defined and clearly shows that oxaliplatin retains the [dach] ligand upon binding to the protein. A water molecule complete the coordination sphere of the Pt centre. Retention of the dach ligand of oxaliplatin is observed during binding to model peptides in other studies [39]. These results are also in line with the experimental observation by Shoeib and coworkers that β-alanyl-L-histidine dipeptide (carnosine) is able to bind oxaliplatin inhibiting its cytotoxic action [39]. Notably, the occupancy factor for the oxaliplatin fragment is = 0.8 in both A and B chains, but its orientation is different in the two molecules: indeed, the dach moiety is exposed to the solvent in molecule A, whereas it orients toward the active site in molecule B. In both cases, an extensive network of hydrogen bonds stabilizes the binding.

Figure 4

In the second binding site (Figure 4C and D), the Pt(II) ion is coordinated to SD atom of Met29, as for RNase A-cisplatin [15] and RNase A-carboplatin adducts. Furthermore, in both molecules

A and B, beyond the SD atom of Met29, Pt also coordinates to OD2 atom of Asp14. Residual Fo-Fc electron density map in this site indicates a possible variability in the anchoring mode of oxaliplatin also close to Met29 and Asp14 side chains. Platination induces a disordering of residues 16-23 in molecule A and 18-21 in molecule B. The occupancy factor for the oxaliplatin fragment (Figure 4C and D) in this site is = 0.4 in molecule A and = 0.6 in molecule B. The relatively low occupancy of the oxaliplatin fragment in molecule A does not allow the modelling of the dach moiety (Figure 4C).

Finally, a minor binding site has been observed close to His105 (Figure 4 E and F). In this site only the Pt atom with occupancy = 0.20 has been modelled.

3.2 ESI MS measurements

A further validation of the proposed RNase A-Pt ligation patterns and of the above interpretation of the electron density maps was achieved by performing independent ESI MS measurements on Pt drug-protein adducts according to the established experimental procedure developed in our laboratory (see Materials and Methods section) (Figure 5). ESI MS spectra were recorded for RNase A-oxaliplatin (Figure 5A), RNase A-carboplatin (Figure 5B), and also for RNase A-cisplatin adducts (Figure 5C).

Inspection of mass spectrometry results provides evidence for the formation of a variety of Pt adducts of different nature, in considerable amounts.

In all cases, monometalated adducts are preferentially formed, though appreciable amounts of bis metalated derivatives are seen, especially in the case of oxaliplatin.

Oxaliplatin forms, at first, two kinds of derivatives, of mass 13988.3 and 14078.3 Da, in comparable amounts, assignable respectively to bidentate and monodentate species (Figure 5A); with time, the relative abundance of the bidentate adduct become higher and predominant on monodentate adduct, with associated release of oxalate ligand. In analogy with oxaliplatin, carboplatin (Figure 5B), first, forms a predominant monodentate derivative; for longer incubation times the cyclobutane-1,1-dicarboxylate ligand (CBD) is progressively released and a peak assignable to the bidentate adduct increases in intensity. Though of low intensity, a peak falling at 14423.4 Da, is representative for bis-adduct formation.

Comparative analysis of peak intensities for the metal-protein adducts suggests that oxaliplatin and cisplatin (Figure 5C) are far more reactive than carboplatin, although differing ionization efficiencies may also be a contributing factor.

Figure 5

4. Discussion

We have reported here the X-ray structures of the RNase A-carboplatin and RNase A-oxaliplatin adducts. As the crystal structure of the RNase A-cisplatin had been previously solved [15], we are in the fortunate position that structures are now available for RNase A adducts with the three main Pt drugs; this allows making instructive structural comparisons. Notably, such an analysis is carried out using structures obtained by soaking metallodrugs into pre-existing isomorphous RNase A crystals grown under very similar conditions. The finding that the RNase A crystals

contain two molecules in the asymmetric unit adds an internal validation to our results. Moreover, the crystallographic investigation has been nicely complemented by ESI MS data on the same adducts which support the correct identification of the Pt species bound to the protein. The importance of using two independent biophysical methods such as X-ray crystallography and ESI MS on the same system is thus further documented [41-42] and underscored. In particular, ESI MS data turn very valuable in elucidating the nature of protein bound platinum fragments for the RNase A-carboplatin adduct where crystallographic data are ambiguous, whereas X-ray diffraction data add molecular details on the binding of oxaliplatin to the protein. The results of this comparative structural analysis are summarized in Table 1. On the basis of the reported data, the following considerations can be done:

-cisplatin and carboplatin behave in a similar way, as they both produce, under the applied experimental conditions, a monometalated protein derivative where the Pt ion of the drug fragment mainly coordinates to SD atom of Met29. The platinum fragment coordinated to Met29 is distinct for the two drugs: it is $[Pt(NH_3)_2]^{2+}$ for cisplatin and $[Pt(NH_3)_2CBD]$ for carboplatin. Analyzing the metal binding site of carboplatin and cisplatin in detail, minor differences are observed that are probably due to the different steric hindrance of the Pt ligands. In the molecule B of the RNase A-cisplatin adduct [15], Pt can coordinate both SD atom of Met29 and NE atom of Gln28 (bidentate interaction)[15], whereas only a monodentate interaction with Met29 seems to occur for carboplatin. Notably, ESI MS results performed after a long incubation time point out that the CBD ligand may be released, so that a type of Pt fragment identical to that arising from cisplatin is eventually associated with the protein, and that a dimetalated adduct can also be formed. In addition, it must be stressed that cisplatin shows a greater reactivity than carboplatin in terms of amounts of formed derivatives as well witnessed by ESI MS results.

Table 1

Oxaliplatin also binds Met29, but it coordinates RNase A through interaction of a $[Ptdach]^{2+}$ fragment. Furthermore, a bidentate coordination is observed that involves the OD1 atom of Asp14. The result confirms previous observations obtained with HEWL in which coordination of the $[Ptdach]^{2+}$ cation selectively occurs at the level of the free carboxylate group of Asp residues [24]. ESI MS data suggest that the binding of oxaliplatin to the protein could occur according to a two-step process. Combining our data with the mechanism proposed for the acid hydrolysis of oxaliplatin [43-44], a picture of the RNase A-oxaliplatin recognition can be drawn: the oxalate ligand of Pt is detached in two consecutive steps, which involve the formation of oxalate monodentate complex. The ring-opening step allows the replacement of oxalate with the carboxylate from the Asp residue (Figure 6). Ring-opened Met adducts of carboplatin have been studied previously [45]. Since the formation of hydrolysis product species has been observed in vivo [43-44], this mechanism could be operative also under physiological conditions.

Figure 6

Notably, in the RNase A-oxaliplatin adduct, other Pt binding sites are also detected. In the main binding site, Pt coordinates the ND1 atom of His119. Furthermore, oxaliplatin can also bind, with low occupancy, the NE2 atom of His105. These results are interesting since it has been previously shown, by studying its interaction with HEWL, that oxaliplatin preferentially binds

Asp side chains [24], while both carboplatin and cisplatin show a preference for His side chains [12, 46]. This is even more surprising if one takes into account that the oxaliplatin fragment bound to RNase A is larger than those of carboplatin and cisplatin. These results could be explained by considering the kinetics of the protein-metallodrug recognition. In fact, it has been shown that, contrary to its DNA binding capacity, the rate of protein binding of oxaliplatin may be significantly higher than that of cisplatin and carboplatin [7, 47]. On the other hand, these data also agree with previous crystallographic findings on the adduct formed in the reaction between trans-Pt derivatives and RNase A [26]. It should be also noted that cisplatin has been found to bind both His105 and His119 in RNase A-cisplatin crystals of a different space group and obtained under different crystallization conditions [25]. In this respect, we cannot exclude that carboplatin could be able to bind His105 and His119, using the approach described in reference 25 or after longer soaking time.

5. Conclusions

The results of this comparative structural analysis suggest that cisplatin and carboplatin behave similarly when they react with proteins, while oxaliplatin shows a significantly different behavior. We suggest that differences in reactivity and adduct formation with proteins, which could be related to a different kinetics of metallodrug-protein binding, may have a more general significance and may be at the basis of the different pharmacological and toxicological profile of the three drugs. Altogether these data support previous hypotheses that metal ligands play a key role in the protein-metallodrug interactions, driving the drug-biological target recognition and stabilizing the structure of the final adduct [48]. The binding of cisplatin, carboplatin and oxaliplatin to Met appears also interesting if one considers that Pt binding to S-donor ligands,

including methionine and glutathione, occur in physiological conditions and that it plays a relevant role in the Pt-drugs metabolism. S-donor binding of Pt-drugs was suggested to be involved as an intermediate in transport to the DNA in nucleus [48-51]. Finally, our data point out that the three Pt drugs mainly bind proteins through formation of monodentate (like carboplatin or cisplatin in molecule A [15]) or bidentate (like oxaliplatin, or cisplatin in molecule B [15]) derivatives.

Before binding, the Pt complex needs to be activated. Activation consists of the release of labile ligands: two chlorides in the case cisplatin, the cyclobutandicarboxylate ligand in the case of carboplatin; oxalate in the case of oxaliplatin. The activation process and the consequent protein metalation may manifest a large kinetic variability depending on the nature of the leaving group and on the possible "assistance" offered by the protein.

Acknowledgments

We gratefully acknowledge Beneficentia Stiftung and COST Action CM1105 for financial support. The authors thank G. Sorrentino, M. Amendola (CNR Institute of Biostructures and Biomages, Naples) for technical assistance and CISM, University of Florence, for recording of ESI-MS spectra.

References

[1] Wang, D.; Lippard, S.J. Nat. Rev. Drug Discov. 4 (2005) 307-320.

[2] Rabik, C.A.; Dolan, M.E. Cancer Treat. Rev. 33 (2007) 9-23.

[3] Brabec, V. Prog. Nucleic Acid Res. Mol. Biol. 71 (2002) 1-68.

[4] Reedijk, J. Proc. Natl. Acad. Sci. 100 (2003) 3611-3616.

[5] Casini, A.; Gabbiani, C.; Mastrobuoni, G.; Messori, L.; Moneti, G.; Pieraccini, G. Chem. Med. Chem. 1 (2006) 413-417.

[6] Graham, M.A.; Lockwood, G.; Greenslade, D.; Brienza, S.; Bayssas, M.; Gamelin, E. Clinical Cancer Research 6 (2000) 1205-1218.

[7] Raymond, E.; Faivre, S.; Chaney, S.; Woynarowski, J.; Cvitkovic, E. Mol. Cancer Ther. 1 (2002) 227-235.

[8] Pinato, O.; Musetti, C.; Sissi, C. Metallomics 6 (2014) 380-395.

[9] Pil, P.; Lippard, S.J. Encyclopedia of Cancer, Vol. 1 [Ed: J.R. Bertino], Academic Press: San Diego, CA, 1997, pp. 392-410.

[10] Arnesano, F.; Natile, G. Pure Appl. Chem. 80 (2008) 2715-2725.

[11] Casini, A.; Reedijk, J. Chemical Science 3 (2012) 3135-3144.

[12] Casini, A.; Mastrobuoni, G.; Temperini, C.; Gabbiani, C.; Francese, S.; Moneti, G.; Supuran, C.T.; Scozzafava, A.; Messori, L. Chem. Commun. 2 (2007) 156-158.

[13] Boal, A.K.; Rosenzweig, A.C. J. Am. Chem. Soc. 131 (2009) 14196-14197.

[14] Calderone, V.; Casini, A.; Mangani, S.; Messori, L.; Orioli, P.L. Angew. Chem. Int. Ed. Engl. 45 (2006) 1267-1269.

[15] Messori, L.; Merlino, A. Inorg. Chem. 53 (2014) 3929-3931.

[16] Banci, L.; Bertini, I.; Blazevits, O.; Calderone, V.; Cantini, F.; Mao, J.; Trapananti, A.; Vieru, M.; Amori, I.; Cozzolino, M.; Carrì, M.T. J. Am. Chem. Soc. 134 (2012) 7009−7014.

[17] Ferraro, G.; Messori, L.; Merlino, A.; Chem Commun. 51 (2015) 2559-2561.

[18] Huliciak, M.; Reinhard, L.; Laursen, M.; Fedosova, N.; Nissen, P.; Kubala M. Biochem. Pharmacol. 92 (2014) 494-498.

[19] Ferraro, G.; Massai, L.; Messori L.; Merlino, A. Chem Commun. 51 (2015) 9436-9439.

[20] Sadler, P.J.; Benz, F.W.; Roberts, G.C.K. Biochim. Biophys Acta 359 (1974) 13-21.

[21] Helliwell, J.R.; Tanley, S.W.M. Acta Cryst. D69 (2013) 121-125.

[22] Tanley, S.W.M.; Schreurs, A.M.M.; Kroon-Batenburg, L.M.J.; Helliwell, J.R. Acta Cryst. F68 (2012) 1300-1306.

[23] Helliwel, J.R.; Tanley, S.W.M. Acta Cryst. F70 (2014) 1127-1131.

[24] Messori, L.; Marzo, T.; Merlino, A. Chem. Commun. 50 (2014) 8360-8362.

[25] Picone, D.; Donnarumma, F.; Ferraro, G.; Russo Krauss, I.; Fagagnini, A.; Gotte, G.; Merlino, A. J. Inorg. Biochem. 146 (2015) 37-43.

[26] Messori, L.; Marzo, T.; Michelucci, E.; Russo Krauss, I.; Navarro-Ranninger, C.; Quiroga, A.G.; Merlino, A. Inorg. Chem. 53 (2014) 7806-7808.

[27] Vergara, A.; Montesarchio, D.; Russo Krauss, I.; Paduano, L.; Merlino, A. Inorg. Chem. 52 (2013) 10714-10716.

[28] Messori, L.; Scaletti, F.; Massai, L.; Cinellu, M.A.; Russo Krauss, I.; di Martino, G.; Vergara, A.; Paduano, L.; Merlino, A. Metallomics 6 (2014) 233-236.

[29] Raines, R.T. Chem Rev. 98 (1998) 1045-1065.

[30] Russo Krauss, I.; Sica, F.; Mattia, C.A.; Merlino, A. Int. J. Mol. Sci. 13 (2012) 3782-3800.

[31] Messori, L.; Merlino, A. Dalton Trans. 43 (2014) 6128-6131.

[32] Messori, L.; Cinellu, M.A.; Merlino, A. ACS Med. Chem. Letters 5 (2014) 1110-1113.

[33] Russo Krauss, I.; Messori, L.; Cinellu, M.A.; Marasco, D.; Sirignano, R.; Merlino, A. Dalton Trans. 43 (2014) 17483-17488.

[34] Otwinowski, Z.; Minor, W. Methods Enzymol. 276 (1997) 307-326.

[35] Vitagliano, L.; Merlino, A.; Zagari, A.; Mazzarella, L. Proteins 46 (2002) 97-104.

[36] Murshudov, N.; Skubak, P.; Lebedev, A.A.; Pannu, N.S.; Steiner, R.A.; Nicholls, R.A.; Winn, M.D.; Long, F.; Vagin, A.A. Acta Cryst. D67 (2011) 355-367.

[37] Emsley, P.; Cowtan, K. Acta Cryst. D60 (2004) 2126-2132.

[38] Laskowski, R. A.; Macarthur, M. W.; Moss, D. S.; Thornton, J. M. J. Appl. Cryst. 26 (1993) 283-291.

[39] Moustafa, E. M.; Camp, C. L.; Youssef, A. S.; Amleh, A.; Reid, H. J.; Sharpb, B. L.; Shoeib, T. Metallomics 5 (2013) 1537-1546.

[40] Shoeib, T.; Sharp, B. L. Metallomics 4 (2012) 1308-1320.

[41] Messori, L.; Marzo, T.; Gabbiani, C.; Alvarez-Valdez, A.; Quiroga, A.G.; Merlino, A. Inorg. Chem. 52 (2013) 13827-13829.

[42] Messori, L.; Marzo, T.; Sanches, R.N.; Hanif-Ur-Rehman, de Oliveira Silva, D.; Merlino, A. Angew. Chem. Int. Ed. Engl. 53 (2014) 6172-6175.

[43] Lucas, M.F.A.; Pavelka, M.; Alberto, M.E.; Russo, N. J. Phys. Chem. B 113 (2009) 831-838.

[44] Luo, F.R.; Wyrick, S.D.; Chaney, S.G. Cancer Chemother. Pharmacol. 44 (1999) 29-38.

[45] Barnham, K.J.; Frey, U.; Murdoch, P.S.; Ranford, J.D.; Sadler, P.J.; Newell, D.R. J. Am. Chem. Soc. 116 (1994) 11175-11176.

[46] Marasco, D.; Messori, L.; Marzo, T.; Merlino, A. Dalton Trans. 44 (2015) 10392-10398.

[47] Pendyala, L.; Creaven, P.J. Cancer Research 53 (1993) 5970-5976.

[48] Lempers, E.L.M.; Inagaki, K.; Reedijk, J.; Inorg. Chim. Acta 152 (1988) 3, 201-207.

[49] Li, C.; Li, Z.; Sletten, E.; Arnesano, F.; losacco, M.; Natile, G.; Liu, Y. Angew. Chem. Int. Ed. Engl. 48 (2009) 8497-8500.

[50] van Boom, S.S.G.E.; Reedijk, J. J. Chem. Soc., Chem. Commun. (1993) 1397-1398.

[51] Lempers, E.L.M.; Reedijk, J. Inorg. Chem. 29 (1990) 217-222.

Table 1. Structural features of Pt-drug binding sites from the X-ray structures of the adducts obtained by soaking procedure on C2 crystals of RNase A and by ESI MS data

Pt drug	RNase A binding sites as revealed by X-ray structural analysis of the adducts obtained by soaking procedure*	Number of binding sites	Binding mode suggested by X-ray structural analysis	Drug Fragment suggested by X-ray structural analysis	Drug Fragment as revealed by ESI MS
Cisplatin**	Mol A: Met29 Mol B: Met29, Gln28	1	monodentate bidentate	$[Pt(NH_3)H_2O]^{2+}$ $[Pt(NH_3)_2]^{2+}$	$[Pt(NH_3)Cl]^{+}$ $[Pt(NH_3)_2]^{2+}$
carboplatin	Mol A: Met29 Mol B: Met29	1	monodentate monodentate	undefined undefined	$[Pt(NH_3)_2]^{2+}$ $[Pt(NH_3)_2CBD]$ $2[Pt(NH_3)_2CBD]$
oxaliplatin	Mol A: His119 Met29, Asp14 His105 Mol B: His119 Met29, Asp14 His105	3	monodentate bidentate monodentate monodentate bidentate monodentate	$[Pt(dach)(H_2O)]^{2+}$ $[Pt(dach)]^{2+}$ undefined $[Pt(dach)(H_2O)]^{2+}$ $[Pt(dach)]^{2+}$ undefined	Oxaliplatin $[Pt(dach)]^{2+}$ Oxaliplatin +$[Pt(dach)]^{2+}$ $2[Pt(dach)]^{2+}$

*It is interesting to note that all RNase A residues involved in the three platinated adducts (Asp14, Gln28, Met29, His105 and His119) are conserved in the human pancreatic enzyme (HP-RNase).

**from reference 15

Figure legends

Figure 1. Structure of cisplatin, carboplatin and oxaliplatin

Figure 2. Ribbon representation of the asymmetric unit of the RNase A-cisplatin (panel A), RNase A-oxaliplatin (panel B) and RNase A-carboplatin (panel C) structures. The molecules A and B are coloured in cyan and purple, respectively. Side chains of residues involved in the Pt drugs recognition are shown along with Pt centres. In panel B and C, 2Fo-Fc electron density maps are coloured in red and contoured at 4σ. The structures of RNase A-oxaliplatin and RNase A-carboplatin have been deposited in the Protein Data Bank with entry codes 4S18 and 4S0Q. The structure of RNase A-cisplatin was already solved and deposited in the PDB with entry code 4OT4.

Figure 3. Details of the binding sites of Pt(II) in the RNase A-Carboplatin adduct. Pt ion is bound to Met29 in the molecule A (panel A) and B (panel B). Asp14 side chain is included in the figure, since it is involved in the recognition of oxaliplatin (see below). 2Fo-Fc electron density maps are contoured at 0.8σ level (grey) and 4.0σ level (red).

Figure 4. Details of the binding sites of Pt(II) in the RNase A-oxaliplatin structure. The drug is bound to protein through a coordinative interaction with side chain of His119 (panel A and B for molecules A and B, respectively). The $[Ptdach]^{2+}$ fragment is involved in a number of hydrogen bonding interactions with water molecules that form an intricate network stabilizing the structure. Furthermore, Pt ion is bound to Met29 and Asp14 side chains (panel C and D for

molecules A and B, respectively). Oxaliplatin binding to sulfur atoms of physiologically important molecules like glutathione has been already observed in other studies [39]. Finally, a minor Pt binding site has been identified close to side chain of His105 (panel E and F for molecules A and B, respectively). 2Fo-Fc electron density maps are contoured at 0.8σ level (grey) and 4.0σ level (red). Molecule A is coloured in cyan and molecule B in purple. In panels C, E and F only the atoms included in the final models are reported, for this reason in panel C some atoms of dach fragment are omitted, whereas in panels E and F only the Pt atoms are reported.

Figure 5. Deconvoluted ESI MS spectra of RNase A treated respectively with $3*10^{-4}$ M of oxaliplatin (panel A), carboplatin (panel B) and cisplatin, (CDDP, panel C) recorded after 24h (A), 72h (B), 168h (C) of incubation at 37 °C. Experimental conditions: Metal:protein ratio = 3:1; buffer: 20 mM ammonium acetate pH 6.8.

Figure 6. Proposed mechanism for oxaliplatin hydrolysis and binding to Met29 and Asp14 residues of RNase A. The bidentate adduct formation proceeds through ring opening and initial formation of a monodentate intermediate.

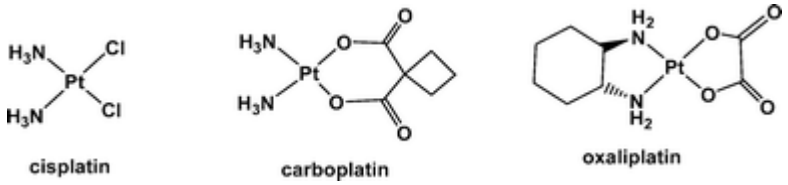

Figure 1. Structure of cisplatin, carboplatin and oxaliplatin

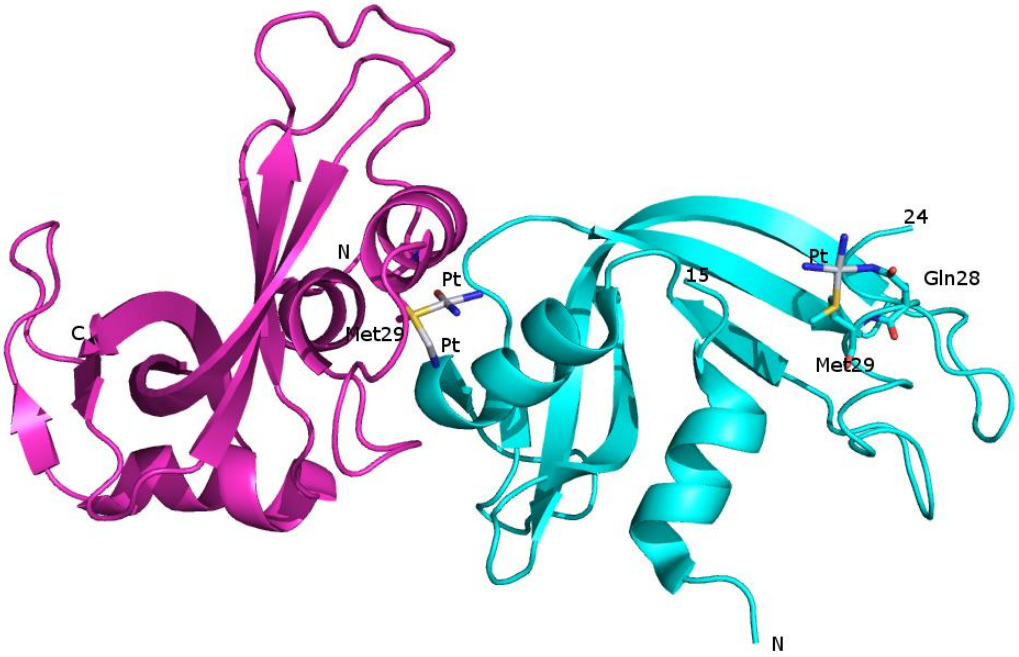
N
Pt
Met29
Pt
C
24
Pt
15
Gln28
Met29
N

A

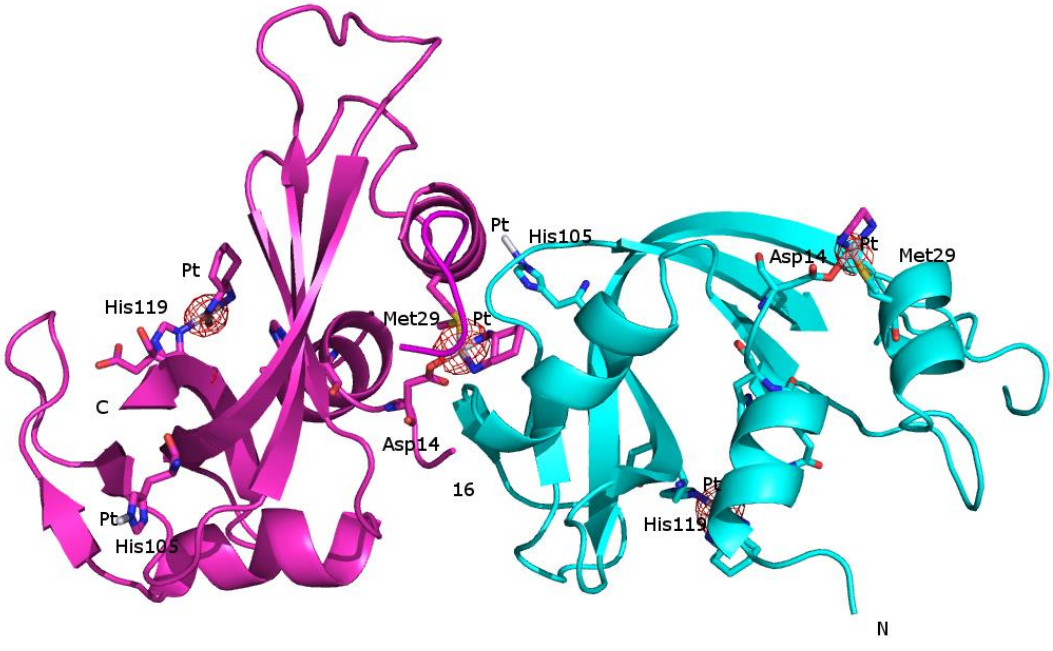
Pt
His105
Pt
Asp14
Pt
Met29
His119
Met29
Pt
C
Asp14
16
Pt
His119
Pt
His105
N

B

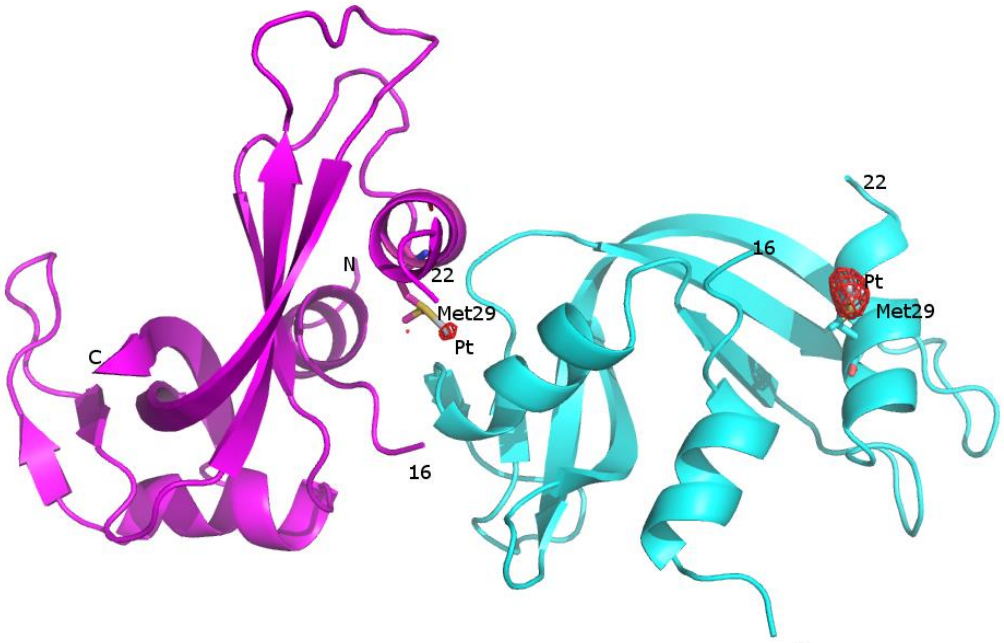

C

Figure 2. Ribbon representation of the asymmetric unit of the RNase A-cisplatin (panel A), RNase A-oxaliplatin (panel B) and RNase A-carboplatin (panel B) structures. The molecules A and B are coloured in cyan and purple, respectively. Side chains of residues involved in the Pt drugs recognition are shown along with Pt centres. In panel B and C, 2Fo-Fc electron density maps are coloured in red and contoured at 4σ. The structures of RNase A-oxaliplatin and RNase A-carboplatin have been deposited in the Protein Data Bank with entry codes 4S18 and 4S0Q. The structure of RNase A-cisplatin was already solved and deposited in the PDB with entry code 4OT4.

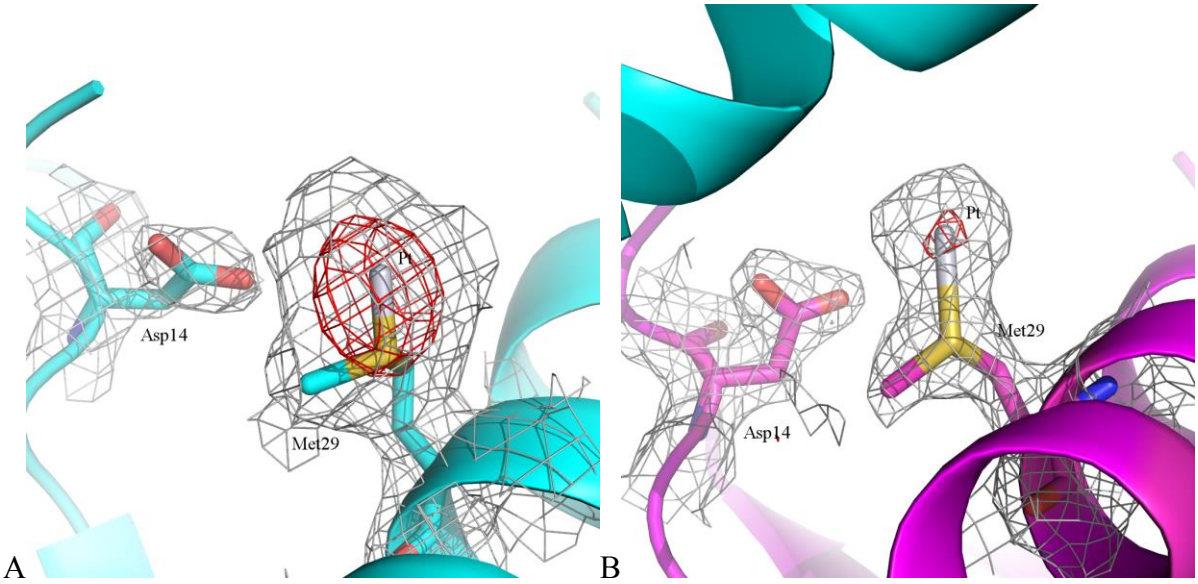

Figure 3. Details of the binding sites of Pt(II) in the RNase A-Carboplatin adduct. Pt ion is bound to Met29 in the molecule A (panel A) and B (panel B). Asp14 side chain is included in the figure, since it is involved in the recognition of oxaliplatin (see below). 2Fo-Fc electron density maps are contoured at 0.8σ level (grey) and 4.0σ level (red).

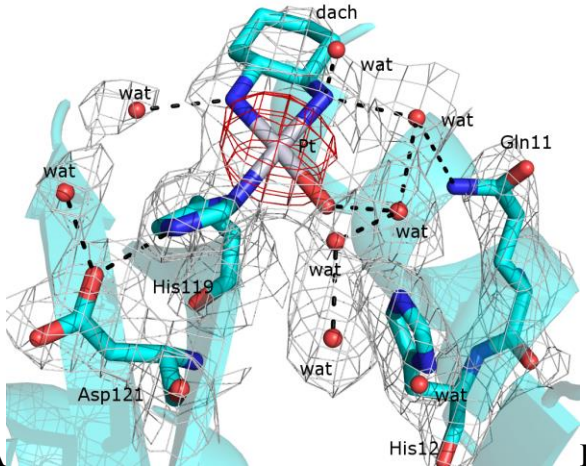
dach
wat
wat
wat
Pt
Gln11
wat
wat
wat
His119
wat
wat
Asp121
wat
His12

A

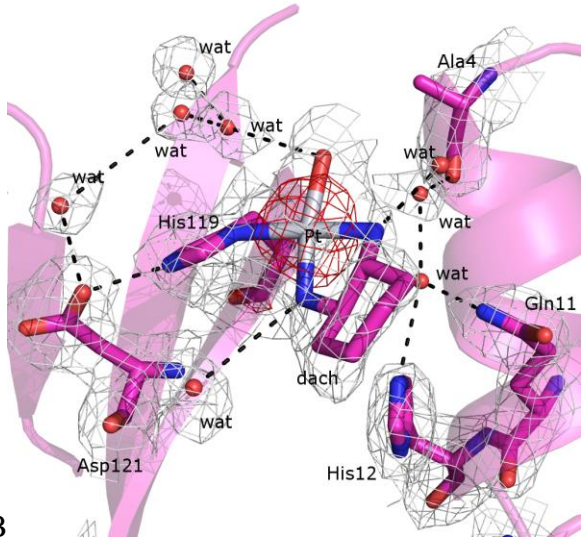
wat
Ala4
wat
wat
wat
wat
His119
Pt
wat
wat
Gln11
dach
wat
Asp121
His12

B

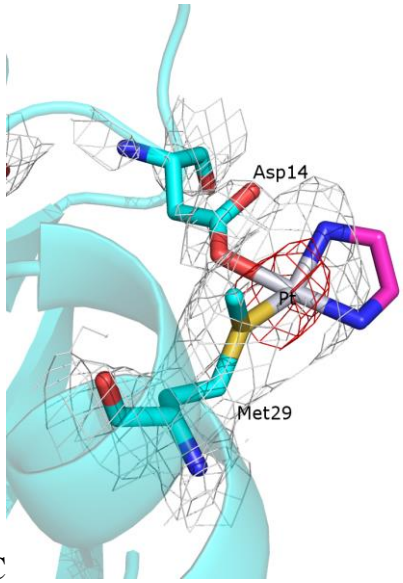
Asp14
Pt
Met29

C

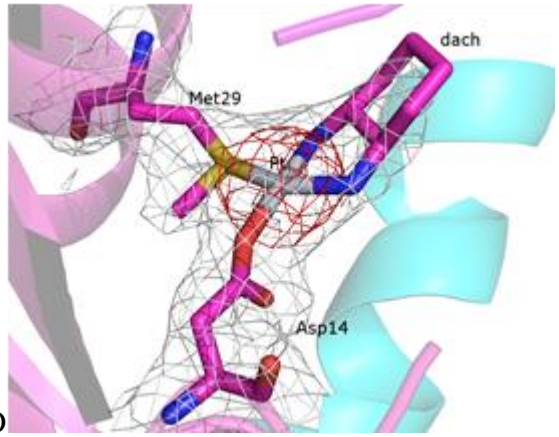
dach
Met29
Pt
Asp14

D

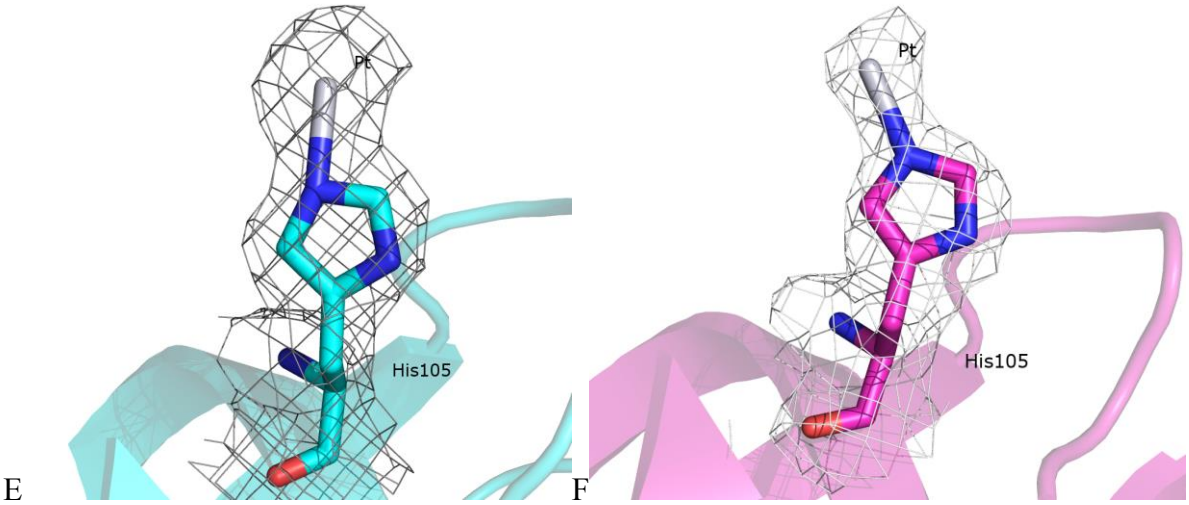

Figure 4. Details of the binding sites of Pt(II) in the RNase A-oxaliplatin structure. The drug is bound to protein through a coordinative interaction with side chain of His119 (panel A and B for molecules A and B, respectively). The $[Ptdach]^{2+}$ fragment is involved in a number of hydrogen bonding interactions with water molecules that form an intricate network stabilizing the structure. Furthermore, Pt ion is bound to Met29 and Asp14 side chains (panel C and D for molecules A and B, respectively). Oxaliplatin binding to sulfur atoms of physiologically important molecules like glutathione has been already observed in other studies [39]. Finally, a minor Pt binding site has been identified close to side chain of His105 (panel E and F for molecules A and B, respectively). 2Fo-Fc electron density maps are contoured at 0.8σ level (grey) and 4.0σ level (red). Molecule A is coloured in cyan and molecule B in purple. In panels C, E and F only the atoms included in the final models are reported, for this reason in panel C some atoms of dach fragment are omitted, whereas in panels E and F only the Pt atoms are reported.

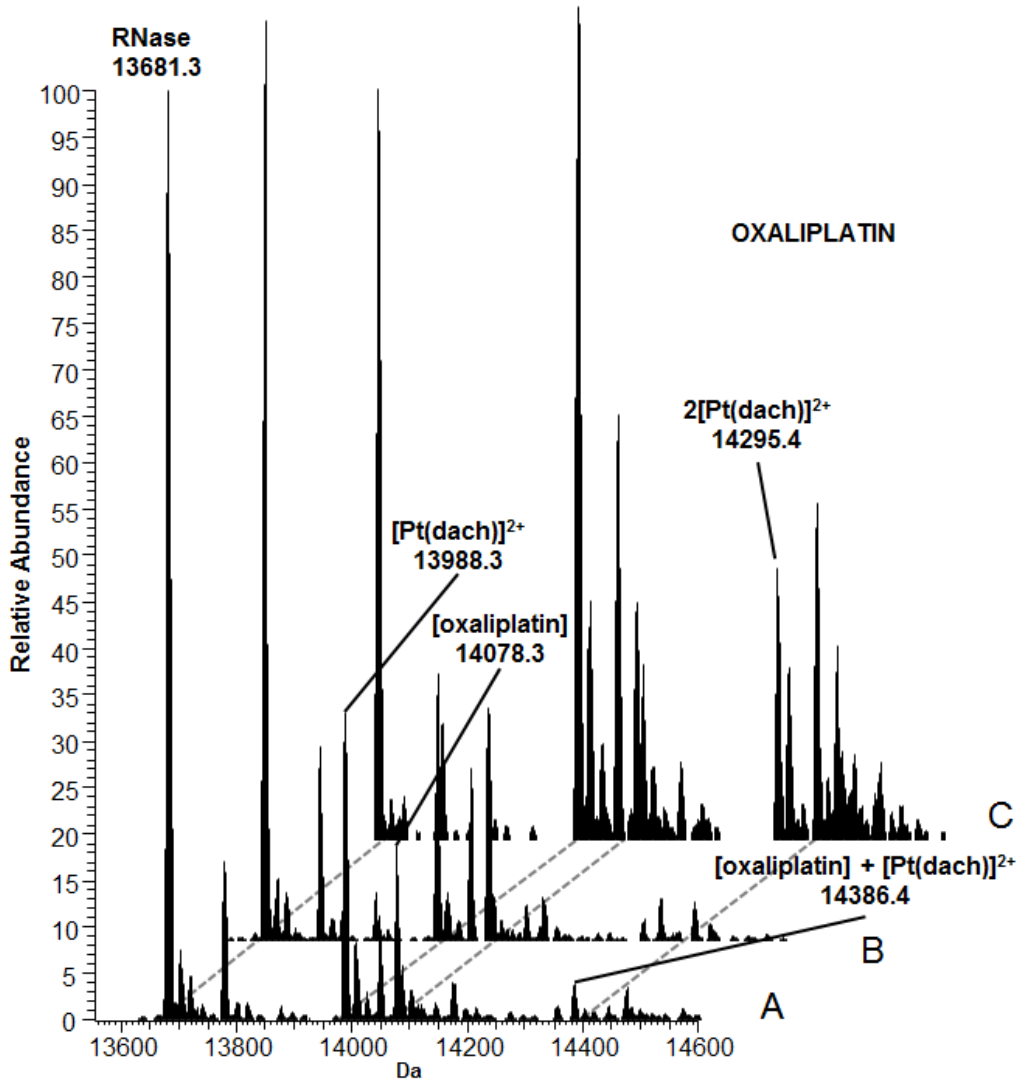
RNase
13681.3
OXALIPLATIN
2[Pt(dach)]2+
14295.4
[Pt(dach)]2+
13988.3
[oxaliplatin]
14078.3
[oxaliplatin] + [Pt(dach)]2+
14386.4
A
B
C
Relative Abundance
Da
100
95
90
85
80
75
70
65
60
55
50
45
40
35
30
25
20
15
10
5
0
13600
13800
14000
14200
14400
14600

A

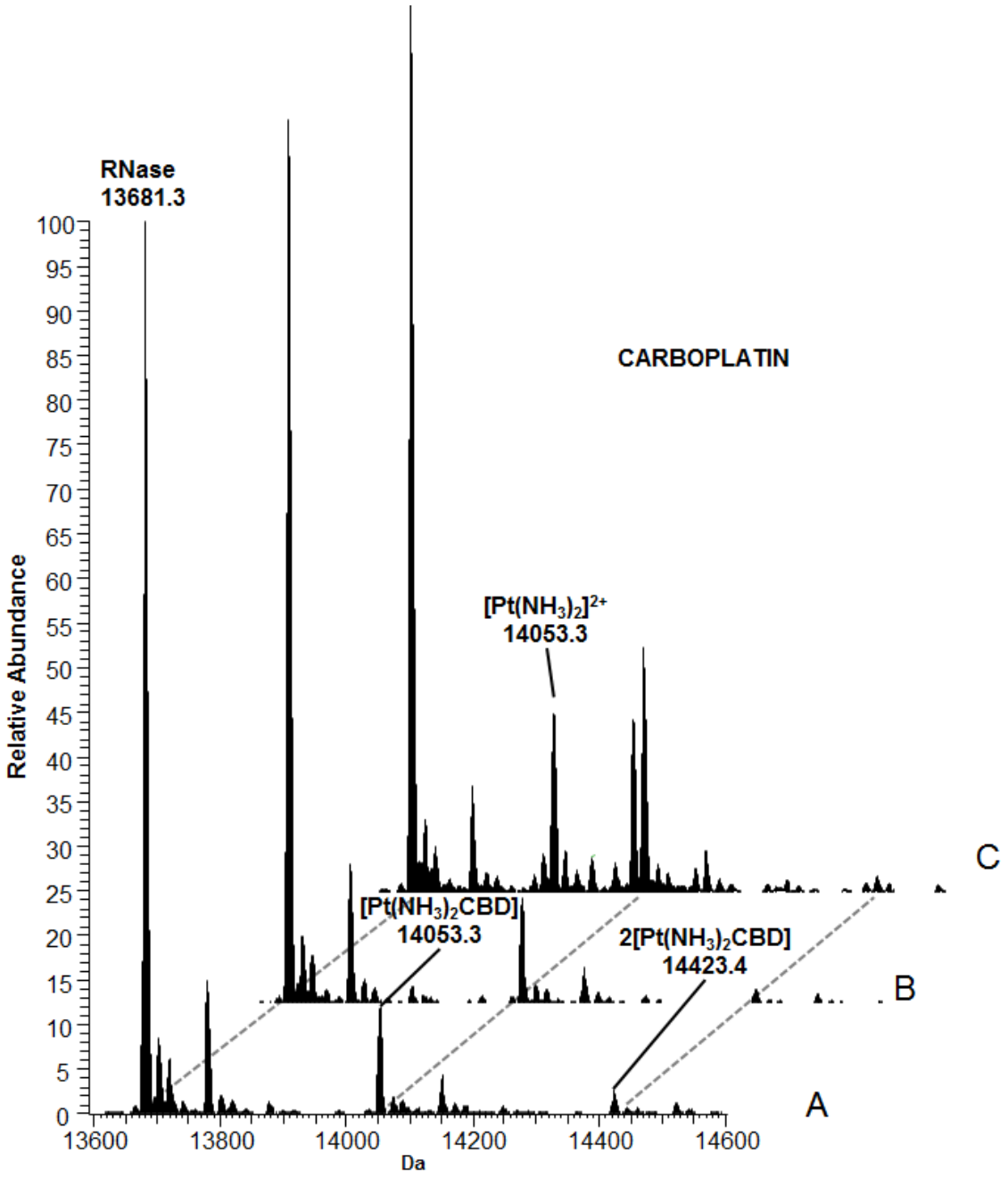
RNase
13681.3
CARBOPLATIN
[Pt(NH3)2]2+
14053.3
[Pt(NH3)2CBD]
14053.3
2[Pt(NH3)2CBD]
14423.4
C
B
A
Relative Abundance
Da
100
95
90
85
80
75
70
65
60
55
50
45
40
35
30
25
20
15
10
5
0
13600
13800
14000
14200
14400
14600

B

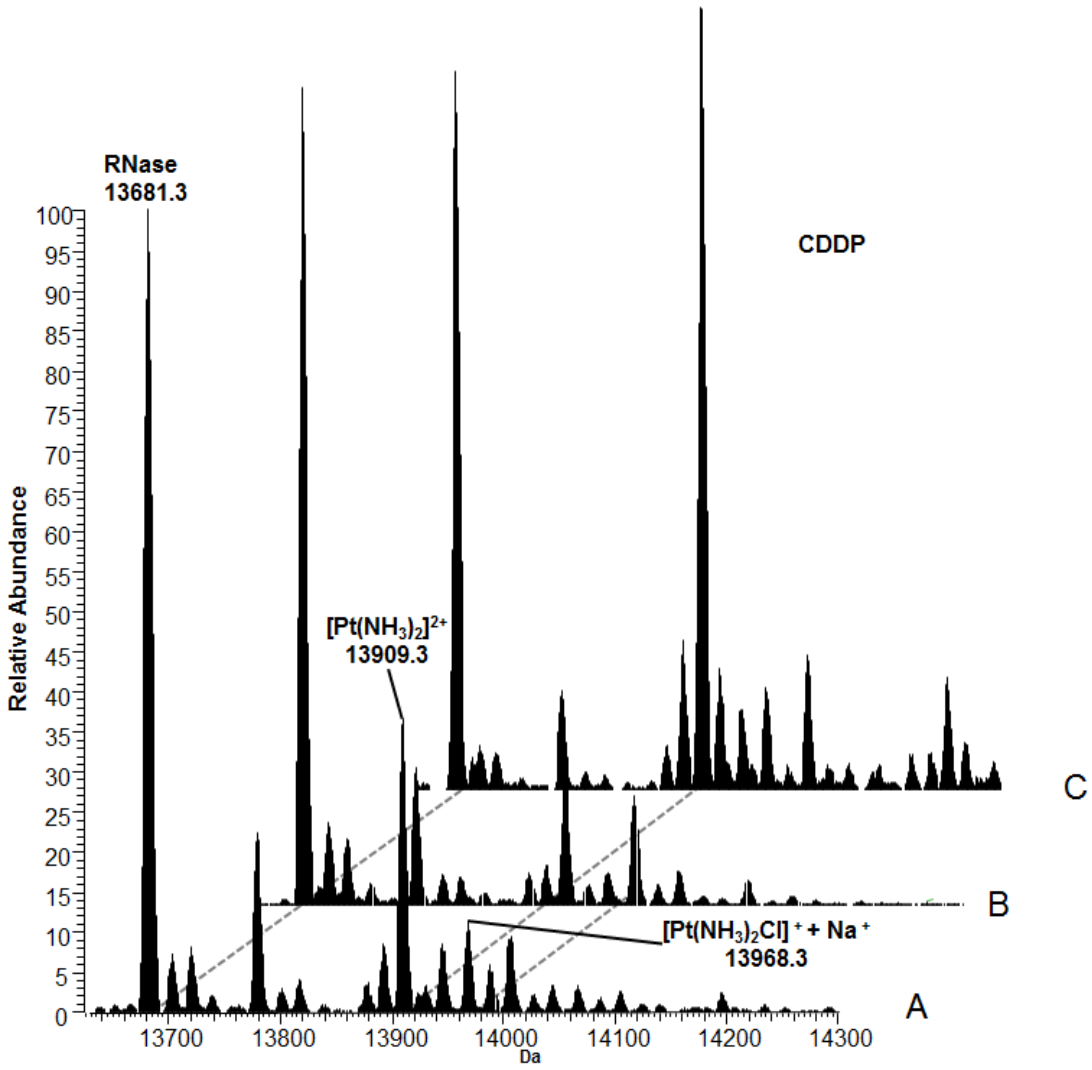

C

Figure 5. Deconvoluted ESI MS spectra of RNase A treated respectively with $3*10^{-4}$ M of oxaliplatin (panel A), carboplatin (panel B) and cisplatin, (CDDP, panel C) recorded after 24h (A), 72h (B), 168h (C) of incubation at 37 °C. Experimental conditions: Metal:protein ratio = 3:1; buffer: 20 mM ammonium acetate pH 6.8.

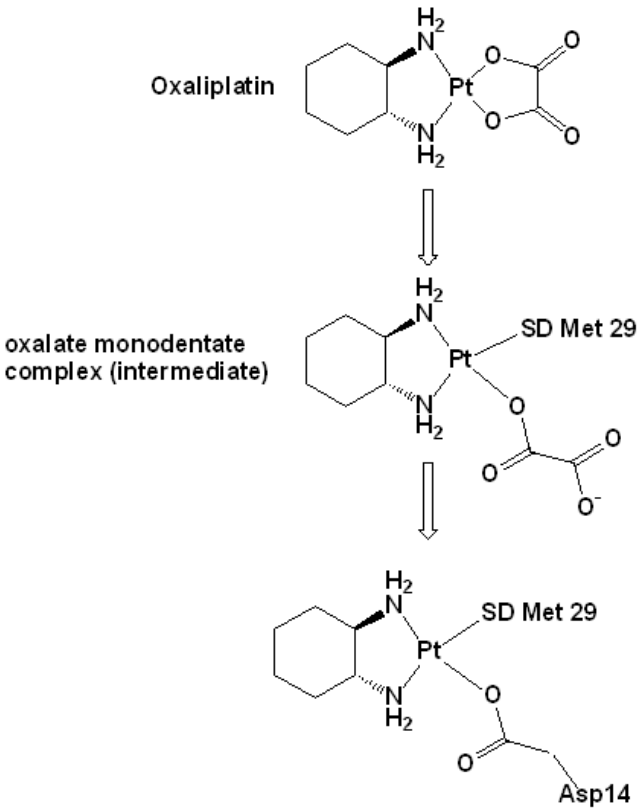

Figure 6. Proposed mechanism for oxaliplatin hydrolysis and binding to Met29 and Asp14 residues of RNase A. The bidentate adduct formation proceeds through ring opening and initial formation of a monodentate intermediate.